Available online at www.sciencedirect.com

ScienceDirect

Procedia CIRP 94 (2020) 239–242

www.elsevier.com/locate/procedia

11th CIRP Conference on Photonic Technologies [LANE 2020] on September 7-10, 2020

Impact of laser irradiation on microstructure and phase development of tungsten carbide - cobalt

Tobias Schwanekamp[a]*, Joachim Gussone[b], Martin Reuber[a]

[a]*Institute of Manufacturing and Tooling Technology (iWFT), University of Applied Sciences (RFH) Cologne, Vogelsanger Str. 295, 50825 Cologne, Germany*
[b]*German Aerospace Center (DLR), Institute of Materials Research, Linder Hoehe, 51147, Cologne, Germany*

* Corresponding author. Tel.: +49-221-54687-743; fax: +49-221-54687-36. *E-mail address:* tobias.schwanekamp@rfh-koeln.de

Abstract

Previous studies on Laser Powder Bed Fusion of tungsten carbide-cobalt (WC-Co) revealed several defects in the laser molten microstructures. To analyze the defect formation mechanisms and the fundamental impact of laser energy input on phase development and microstructure of WC-Co, single-pulse and single-track analogy experiments are conducted. Conventional WC-Co is used as substrate. Variations in cobalt content and processing conditions are investigated. It is found that a single laser exposure can be enough to induce decomposition of microstructure, WC grain growth, formation of non-equilibrium phases and thermal cracking. Based on the results, defect formation mechanisms and countermeasures are discussed.

Keywords: Cemented Carbides, Tungsten Carbide-Cobalt, WC-Co, Laser Melting, Laser Powder Bed Fusion, L-PBF, Non-Equilibrium Phase, Metastable Phase

1. Introduction

Tungsten carbide-cobalt (WC-Co) is widely used for manufacturing of cutting tools. The conventional manufacturing of WC-Co in a liquid phase sintering process is characterized by a well-controlled and homogeneous input of thermal energy and processing times in the order of several hours. Controlled diffusion processes along the grain boundaries between the WC hard phase and the Co binder ensure the formation of the desired material microstructure. After sintering, the solid carbide blanks are contoured using CNC-grinding machines to achieve the final tool shape.

In contrast to the conventional cutting tool fabrication process, Laser Powder Bed Fusion (L-PBF) offers significant potential for manufacturing of innovative tool geometries [1]. However, previous studies indicate that laser molten WC-Co is impaired by characteristic defects, which corrupt the material properties. The laser generated microstructures exhibit increased porosity and WC grain growth, thermal cracks and undesired changes in the composition of elements and phases [1]. A summary of studies conducted on L-PBF of WC-Co at different research institutions was given by Uhlmann et al. [2]. The conditions of melting and solidification during L-PBF are completely different from the conventional liquid phase sintering process. Therefore, microstructure and mechanical properties similar to conventionally sintered WC-Co are still not achieved by L-PBF.

Further optimization requires a better understanding of the defect formation mechanisms. To achieve a more differentiated consideration of the mechanisms, the impact of powder layer characteristics is excluded in this study. Single-pulse and single-track analogy experiments are conducted on conventional solid WC-Co substrate under variation of the cobalt content and the processing conditions. Thereby, the fundamental impact of laser energy input on phase development and microstructure of WC-Co is analyzed. Based on the results, different measures to reduce the material defects are discussed.

10.1016/j.procir.2020.09.045

2. Materials and methods

The experiments were conducted on a Renishaw AM250 L-PBF system under inert gas atmosphere (nitrogen 5.0). The machine is equipped with a modulated Ytterbium fiber laser (cw) with a focal diameter of $d_f = 70$ µm (Gaussian mode, TEM_{00}). Single pulses with pulse durations $t_p \geq 20$ µs can be achieved by modulation. The scan velocity v_S is approximated by $v_S = d_p / t_p$. The local distance d_p between two exposure points is set to a constant value of $d_p = 45$ µm in all tests. The maximum platform temperature in the standard configuration of the AM 250 machine is limited to 170°C. For the realization of higher platform temperatures, a lab scale pre-heating module is used. This module can heat up a build area of 25 mm width and 50 mm length to approx. $T_{PH} = 800$°C. The temperature can be monitored with thermocouples and pyrometry.

Different conventional WC-Co grades with variations in the Co-content from 6 wt.-% to 24 wt.-% were used. The WC grain size of the tested materials increases with the Co-content from "fine" to "coarse" (classification according to ISO 4499). The surfaces of the samples were ground and polished. Variations in scan velocity (25 mm/s $\leq v_S \leq$ 200 mm/s) and laser power (50 W $\leq P \leq$ 200 W) were chosen according to the process windows of previous studies on L-PBF of WC-Co [2]. For the single-track experiments, the variations in P and v_S result in a specific energy per unit length $E_s = P / v_S$ between 0.25 J/mm $\leq E_s \leq$ 8 J/mm. The range of v_S results in pulse durations $t_p = d_p / v_S$ between 0.225 ms and 1.8 ms ($d_p = 45$ µm), which are applied for the single-pulse experiments. For the single pulses, the chosen range of P and t_p result in a pulse energy $E_p = P \cdot t_p$ between 11.25 mJ $\leq E_p \leq$ 360 mJ.

The heat affected zones were inspected by top view and polished cross sections of the scan tracks. Optical microscopy and scanning electron microscopy (SEM) were applied. Microstructure was investigated by secondary electron (SE) and backscattered electron (BSE) contrast. The proportion of the elements in the heat affected zones provides a clue for possible phases and is measured by energy dispersive X-ray spectroscopy (EDX). To minimize contamination during sample preparation, some of the microstructural areas were ablated using focused ion beam (FIB). Emphasis of the analysis was on the dimensions of the heat affected zones, the formation of microstructure and the occurrence of thermal cracks.

3. Results and discussion

The first single-track experiments were conducted without pre-heating of the substrate. The results indicate a significant impact of laser energy on the given WC-Co microstructure for all tested parameter combinations and materials. The temperature gradient dT/ds along the distance s from the center of the melt pool causes different microstructural zones. These are shown schematically in Fig. 1. In sufficient distance to the melt pool (zone D), the material is unaffected by the laser energy (E_s, E_p). Summarizing the tendencies seen in all parameter settings, the following microstructural observations have been made. Full decomposition of the WC microstructure is observed in the center of the melt pool (zone C), where the highest temperature can be expected. At the border of the melt pool (zone B), WC grain growth is observed. Between the border (B) and the unaffected material (D), a heat affected zone is detected, where increased amounts of W are measured in the Co phase (zone C). The described zones occur for each parameter setting and tested Co-content, but are most obvious for high energy inputs. Therefore, the typical zones are explained in detail by example of the scan track, that was generated with $E_s = 8$ J/mm.

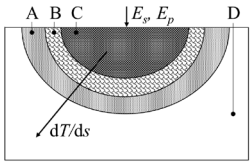

A: heat affected zone, increased saturation of binder phase
B: melt pool border, WC grain growth
C: central melt pool, direct interaction between laser and material, decomposition of carbides
D: unaffected material, original WC-Co microstructure

Fig. 1. Schematic view and description of microstructural zones in the cross section of a laser scan track on WC-Co

Fig. 2 shows the cross-sections of scan tracks generated with WC-Co 76/24 and WC-Co 90/10. Comparison of zone A to the original material in zone D indicates that a significant impact of laser energy input on the carbide structure is not evident. The light-grey WC grains are homogeneously embedded in the dark-grey Co matrix in both regins. However, EDX analysis of this region indicates a gradient in the mole fraction of W (x_W) dissolved in the Co-matrix. In the unaffected zone D a mole fraction of $x_W \approx 1.5$ at.-% is measured. Getting closer to the melt pool, the mole fraction increases up to $x_W \approx 20$ at.-%. This can be explained by the gradient dT/ds, since the solubility of W in Co increases with increasing temperature [3]. The high cooling rates lead to supersaturated solidification. The dissolved tungsten affects the density of the binder phase and thereby the material contrast in the BSE image. For higher Co-contents, filamentary precipitations are observed in the Co-matrix, which are rich in tungsten (detail zone A). These structures suggest not only solid state diffusion but a transition of the binder phase into liquid state. For lower Co-contents, reliable measurement of the mole fraction x_W in the Co matrix was not possible due to the small amount of Co between the WC grains. However, the saturation gradient is visible by the slight decrease in brightness of the binder phase outwards the melt pool. The width of zone A generally increases with the Co-content of the substrate material.

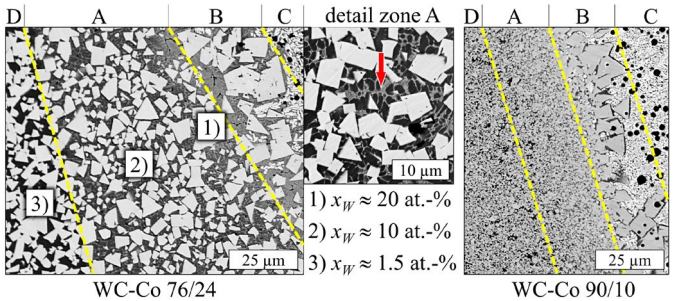

Fig. 2. Scan track cross-sections of zone A (SEM-BSE) with binder phase saturation gradient, $E_s = 8$ J/mm, WC-Co 76/24 (left), WC-Co 90/10 (right)

In the border region B between the central melt pool (zone C) and the heat affected zone A, significant WC-grain growth is observed (Fig. 3). The formation mechanisms are basically known from conventional sintering processes [4]. High temperature leads to increased dissolution of carbides in the liquid binder and a highly saturated melt phase. During solidification and cooling, the dissolved W and C precipitates

at the grain boundaries of the undissolved carbides at the border to zone A, causing grain growth. In addition, the minimization of surface energy leads to partial or full coalescence of grains. In some of the enlarged grains, black inclusions can be identified. These are also observed in the central melt pool and contain high amounts of carbon (Fig. 5). The carbon is enclosed in the WC grains during coalescence and grain growth.

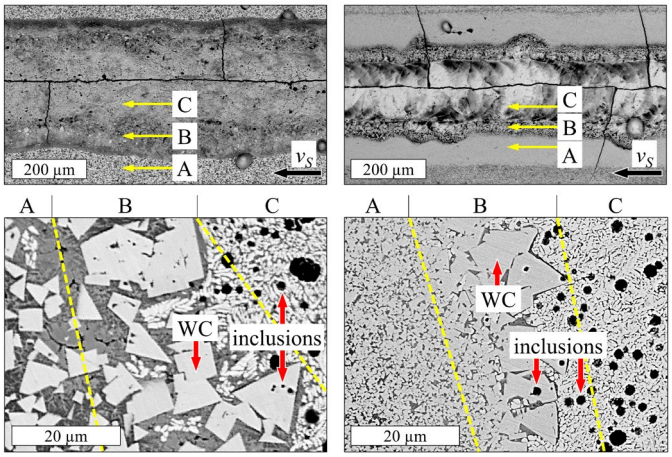

Fig. 3. Scan track top views (top, SEM-BSE) and cross-sections of zone B (bottom, SEM-BSE), E_s = 8 J/mm, WC-Co 76/24 (left), WC-Co 90/10 (right)

In the central interaction zone (C) between the laser radiation and the material, the highest laser intensity, melt pool temperature and temperature gradients exist [5]. Global EDX analysis of these regions is conducted for both Co-contents as shown in Fig. 4 (red frames). The results indicate residual Co contents of approx. 15 wt.-% (WC-Co 76/24) respectively 5 wt.-% (WC-Co 90/10). Hence, a single laser exposure is enough to reduce the initial Co content by up to 50 %. Co evaporation is also known from L-PBF [2]. This indicates, that the evaporation temperature of Co (2900°C) is locally exceeded during laser exposure. According to the W-C-Co phase diagram, given e.g. by Bondar et al. [6], WC is in liquid state at 2900°C. WC melts incongruently, which implies decomposition into W-rich liquid phase and solid graphite (C). Due to rapid cooling, diffusion processes are inhibited. Non-equilibrium conditions can cause meta-stable solidification of the melt. Dependent on the energy input and the Co-content of the substrate, lamellar or cellular microstructures similar to cast material with spheroidal graphite are observed (Fig. 4).

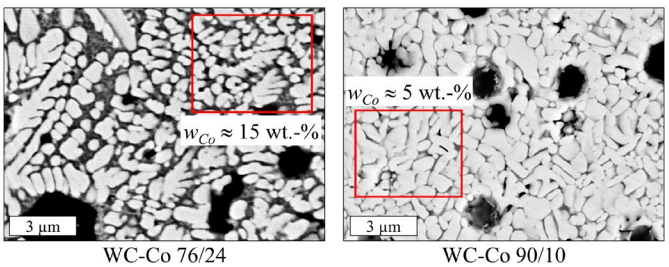

Fig. 4. Scan track cross-sections of zone C (SEM-BSE) with fully decomposed WC, E_s = 8 J/mm, WC-Co 76/24 (left), WC-Co 90/10 (right)

More detailed analysis of this region is conducted by means of EDX mapping on a section prepared by FIB (Fig. 5). Almost 100 % carbon is measured inside the black inclusions. Due to the high cooling rates, the dissolved carbon and tungsten do not precipitate as WC but instead the C remains enclosed in the microstructure as graphite leading to a carbon deficiency in the surrounding material. The light grey regions around the C-inclusions contain high amounts of tungsten. BSE indicates a higher Z-contrast (mean atomic number) and thereby higher material density compared to WC. Hence, potential phases are W_2C, WC_{1-x} (γ) or W. The dark grey matrix is rich in cobalt. The compositions, measured by EDX, most likely suggest supersaturated Co(W,C) or Co_3W.

Microstructures as they are observed in zone C are not known from conventional sintering processes but are sporadically described in beam based surface treatment of hard metal tools. In this context, Xu et al. also confirmed Co-loss due to evaporation and, depending on the energy input, meta-stable phases such as WC_{1-x} and $Co_3W_9C_4$ (κ) [7]. Zhang et al. detected W_3Co_3C (η) and graphite (C), in addition [8].

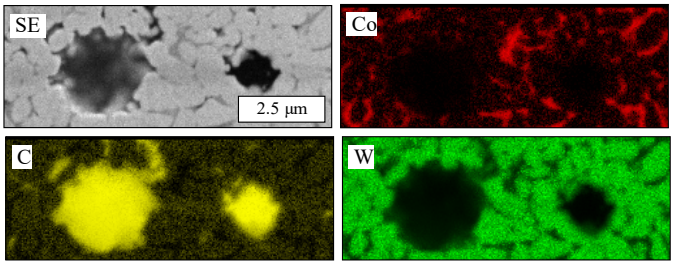

Fig. 5. EDX mapping of the microstructure in the central melt pool region (E_s = 8 J/mm, WC-Co 90/10)

Measurement of the melt pool dimensions indicated, that the width and depth of zone C increase exponentially with the laser energy input. High laser power P ≥ 150 W in combination with low scan velocity v_S < 200 mm/s leads to keyhole effect and keyhole pores. Furthermore, thermal cracks are detected in most of the generated scan tracks. The extent of cracking increases with the induced laser energy. For low E_s, most of the cracks are oriented perpendicular to the scan direction. Additional cracks in longitudinal direction occur for higher E_s. This phenomenon is known from laser welding and is related to the dominating direction of thermally induced tensile stress. Dependent on Young's modulus E, thermal expansion coefficient α, Poisson's ratio ν and temperature difference ΔT, the thermal stress σ_{th} can be approximated by Eq. (1).

$$\sigma_{th} = \frac{E\,\alpha}{1-\nu}\Delta T \tag{1}$$

With increasing Co-content, the Young's modulus of WC-Co hard metals decreases [9], resulting in a decrease of thermal stress. For hard and brittle materials such as WC-Co, rapid transient temperature changes are most critical, since this thermal shock can cause stress peaks, resulting in instant crack initiation and propagation. The thermal shock resistance increases with the fracture toughness K_{IC} of the material [10] and thereby with increasing Co-content and WC-grain size [9]. The experiments indicate that even a single pulse with low energy induces thermal cracking for low Co contents (Fig. 6). The central melt pool region is most prone to crack formation due to the high temperature gradients and the embrittlement caused by Co-evaporation and phase transformation. For low Co-content, additional cracks occur around the melt pool in zone A.

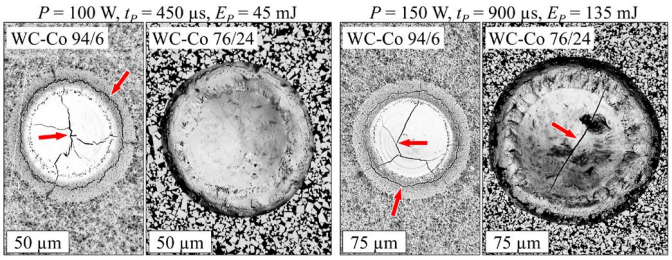

Fig. 6. Single pulses on WC-Co substrate with minimum and maximum Co content and varying pulse energy E_p (top view, SEM-BSE)

The formation of cracks depends on thermal gradients, affected by laser energy input, and on fracture toughness, affected by material ductility. Teppernegg et al. have shown, that the ductility of a given WC-Co composition increases at a temperature around 800°C, resulting in a sudden increase in K_{IC} [11]. An increase in the WC-Co substrate temperature level also reduces ΔT and, according to Eq. (1), the thermal stress. To verify this assumption, similar experiments are conducted at an increased pre-heating temperature $T_{PH} \approx 800$°C. With this temperature, cracks can be prevented in a wide parameter range, even for WC-Co 94/6 and for the highest pulse energy as shown in Fig. 7 (a). With pre-heating, the melt pool dimensions increase. The higher substrate temperature reduces cooling rates. Consequently, it affects the formation of phases. The impact of reduced cooling rates on the microstructure is most distinct for high Co-content as shown in Fig. 7 (b). Taking into account the scheme given in Fig. 1, $T_{PH} \approx 800$°C leads to enlargement of the regions A (solution of W in Co) and B (WC-grain growth). Increased and distorted WC grain growth is observed in zone B for most of the tested parameter settings at $T_{PH} \approx 800$°C. In the central melt pool region (zone C) the lower cooling rates lead to coarser microstructure. Increased porosity is observed in some melt pools, indicating evaporation due to a higher melt pool temperature.

In contrast to the single laser exposure applied in these experiments, the repetitive layer-wise laser exposure during L-PBF increases overall temperature level and reduces cooling rates. Overlapping of scan-tracks, continuous re-melting and re-heating affects the L-PBF-made material below and beside the current track and creates a heterogeneous microstructure, most similar to zone B in the singe-track experiments, as shown in previous studies [1].

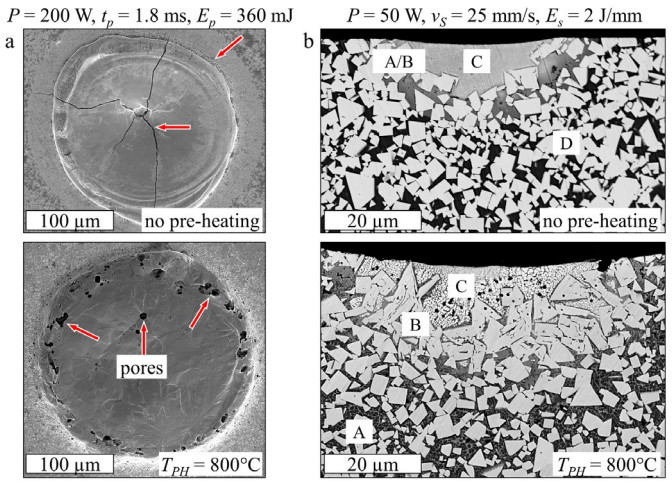

Fig. 7. (a) SEM (SE) images of single pulses on WC-Co 94/6, (b) SEM (BSE) images of single-track cross sections on WC-Co 76/24

4. Conclusion

Single-track and single-pulse experiments on WC-Co with varying Co-content between 6 and 24 wt.-% revealed, that a single laser exposure is already sufficient to induce decomposition of microstructure, WC grain growth, formation of non-equilibrium phases and thermal cracking. The parameter range used in relevant studies on L-PBF of WC-Co [2] was applied. It was found that the decomposition of carbide microstructure in the central interaction zone between the laser beam and the material is inevitable in the tested range of P and v_S. Increased substrate temperature of 800°C reduces thermal gradients and increases material ductility. At $T_{PH} \approx 800$°C, thermal cracking, which is the most critical defect in L-PBF of WC-Co, can successfully be prevented for a wide range of parameters and WC-Co compositions. Melt pool dimensions and heat affected zones are larger at $T_{PH} \approx 800$°C. Consequently, laser energy input and thereby the negative impact on the microstructure should be reduced in the L-PBF process at $T_{PH} \approx 800$°C. Furthermore, the higher temperature level in the substrate leads to enlarged regions with increased saturation of binder. $T_{PH} \approx 800$°C leads to reduction of cooling rates and consequently to increased WC grain growth. Despite these drawbacks, pre-heating is highly recommended for L-PBF of WC-Co to reliably prevent thermal cracking. Beyond a reduction of laser energy input, further measures, such as grain growth inhibitors, additives or alternative binders, should be investigated. For deeper understanding of solidification phenomena and phase development, future research should be supported by thermodynamic simulations and transmission electron microscopy (TEM).

References

[1] Schwanekamp, T. and Reuber, M. (2016) Additive Manufacturing of application optimized tungsten carbide precision tools. in: Proc. 6th Int. Conf. Addit. Technol., Interesansa - zavod, Ljubljana, Nürnberg, Germanypp. 100–114.

[2] Uhlmann, E., Bergmann, A., and Gridin, W. (2015) Investigation on Additive Manufacturing of Tungsten Carbide-cobalt by Selective Laser Melting. *Procedia CIRP*. 35 8–15.

[3] Okamoto, H. (2008) Co-W (Cobalt-Tungsten). *Journal of Phase Equilibria and Diffusion*. 29 (1), 119–119.

[4] Spriggs, G.E. (1995) A history of fine grained hardmetal. *International Journal of Refractory Metals and Hard Materials*. 13 (5), 241–255.

[5] Hooper, P.A. (2018) Melt pool temperature and cooling rates in laser powder bed fusion. *Additive Manufacturing*. 22 548–559.

[6] Bondar, A., Bochvar, N., Dobatkina, T., Krendelsberger, N., Effenberg, G., and Ilyenko, S. (2010) Carbon – Cobalt – Tungsten, Landolt-Börnstein - Group IV Physical Chemistry 11E2 (Refractory metal systems). 41.

[7] Xu, Y., Zhang, Y., Hao, S.Z., Perroud, O., Li, M.C., Wang, H.H., et al. (2013) Surface microstructure and mechanical property of WC-6% Co hard alloy irradiated by high current pulsed electron beam. *Applied Surface Science*. 279 137–141.

[8] Zhang, Y., Yu, F., Hao, S., Dong, F., Xu, Y., Geng, W., et al. (2017) Evolution of Nanostructure and Metastable Phases at the Surface of a HCPEB-Treated WC-6% Co Hard Alloy with Increasing Irradiation Pulse Numbers. *Coatings*. 7 (11), 178.

[9] Spriggs, G.E. (2002) Properties of hardmetals and cermets. in: Powder Metall. Data Refract. Hard Intermet. Mater., Springer, pp. 86–117.

[10] Hasselman, D.P.H. (1969) Unified Theory of Thermal Shock Fracture Initiation and Crack Propagation in Brittle Ceramics. *Journal of the American Ceramic Society*. 52 (11), 600–604.

[11] Teppernegg, T., Klünsner, T., Kremsner, C., Tritremmel, C., Czettl, C., Puchegger, S., et al. (2016) High temperature mechanical properties of WC–Co hard metals. *International Journal of Refractory Metals and Hard Materials*. 56 139–144.